32nd European Modeling & Simulation Symposium
17th International Multidisciplinary Modeling & Simulation Multiconference

ISSN 2724-0029 ISBN 978-88-85741-44-7 © 2020 The Authors.
DOI: 10.46354/i3m.2020.emss.058

Fuzzy Logic-Based Inference System for Prediction of Energy Input in Laser Metal Deposited Aisi316 Single-Beads

Daniel R. Tasé Velázquez [1], André Luís Helleno [2], Maria Célia de Oliveira [1,2], Hipólito Carvajal Fals [3,4], and Emilio Jimenez Macias[5,*]

[1] Post-Graduation Programme in Production Engineering, Methodist University of Piracicaba, São Paulo, Brazil
[2] Engineering School, Mackenzie Presbyterian University, São Paulo, Brazil
[3] College of Mechanical and Industrial Engineering, Oriente University, Santiago de Cuba, Cuba
[4] Visiting Professor at Federal Technological University of Paraná, Paraná, Brazil
[5] Department of Electrical Engineering (DIE), University of La Rioja, Logroño, Spain

*Corresponding author. Email address: emilio.jimenez@unirioja.es

Abstract

Laser metal deposition (LMD) process has the capability to produce functional and complex 3D parts. The deposits characteristics are strongly influenced by the deposition parameters and volume energy input. The aims of this paper is to predict using a fuzzy logic-based inference system (FIS), the volume energy generated after depositing AISI 316 SS single-beads by LMD. Previously to FIS modeling, the influence of laser power (Lp), laser scan speed (Lss), powder flow (Pf) and focal length (Fl) on deposited beads were studied by analyzing the response-variables bead height (Bh) and bead width (Bw). ANOVA allowed identifying that Pf mostly affect the Bh, and Lp has greater significance on Bw. Predictive FIS modeled presented high adequacy assessing the experimental conditions, showing an average relative error of 4.76 %. Thus, the proposed FIS can be can be effectively utilized to predict the volume energy input and be integrated within an automated LMD environment to reduce complexities in process planning activities and increase process stability.

Keywords: additive manufacturing; laser metal deposition; fuzzy logic; volume energy input

1. Introduction

Additive manufacturing (AM) by laser metal deposition (LMD) is an advanced manufacturing process which uses laser as energy source, to build 3D parts melting metallic powders in a layer-by-layer sequence. In LMD additive process, powder is provided so located by a feed nozzle (coaxial) where a flow of inert gas, which may be helium or argon, protects and isolates the material deposition. A metallic powder is completely fused by a laser beam, resulting in highly robust parts. Powder fusion is made by means of a high-power laser directed to impact a substrate, and consecutive layers are deposited to produce the desired object (Schmidt et al. 2017).

LMD process has demonstrated his suitability to produce functional parts with complex geometries which can't be manufactured using conventional processes such as machining or casting. Several works study the development of mostly statistical

approaches for characterizing LMD process parameters assessing different response-variables.

Ansari et al. (2019) studied the iron powder single-tracks geometrical characteristics using laser power, scanning speed and powder feed rate as process parameters by means of RSM (Response Surface Method) and ANOVA (analysis of variance) for testing the regression model.

Wu et al. (2019) developed a laser-powder coupling numerical model for DMD process with discontinuous powder feed rate for simulating the laser attenuation and heat transfer during laser-powder coupling process. Huang et al. (2019) studied the process parameters correlation with the thermal characteristics for microstructure rapid prediction of laser powder-fed additive manufacturing (LPFAM).

Arrizubieta et al. (2018) developed a mathematical model to simulate and predict hardness, grain size and porosity of AISI 304 stainless steel powder deposition through differential equations and Central Finite Difference method.

Yu et al. (2018) studied the process parameters optimization and performance testing of directed laser fabrication. The results showed that laser power, laser scan speed and powder feed rate affect the bead geometry, therefore affect the quality of cladding samples.

Farahmand and Kovacevic (2014), and Liu and Kovacevic (2014) evaluated the effect of laser power, powder feeding rate, scanning speed, carrier-gas flow rate and stand-off distance on the bead geometry, microhardness and powder catchment efficiency using CCD-RSM.

The commonly process parameters studied include, but not limited, laser power, powder flow and feeding-rate, laser velocity scan and stand-off distance between the laser head and substrate. Most of the surveys explore only through statistical analysis, the effect of the process parameters on the geometrical characteristics of deposited layers.

However, one important variable that is highly dependent of process parameters and geometrical characteristics interaction is the energy per volume of material generated during a layer deposition. While much of the reported studies about LMD process parameters performance and its effect on output variables do not include sufficient information to compute the energy inputs, some studies presents different approaches and processes for this analysis.

Thijs et al. (2010) study the microstructural performance during selective laser melting (SLM) of Ti−6Al−4V. One of the variables studied was the effect on the energy density E (J m-3) after using different strategies, such as, varying the hatch spacing and scan velocity.

Amine, Newkirk and Liou (2014) evaluated the influence of laser parameters on the shape and size of the laser melt pool by analyzing the specific energy (Es) involved.

Wei et al. (2014) studied the effect of energy input (laser energy per volume Ev) on formability, microstructure and mechanical properties of deposited AZ91D magnesium-alloy by SLM. The results showed that laser energy input plays a major role on the quality of the samples.

Cherry et al. (2015) used SLM to investigate the effect of laser energy density (Q) in J/mm3, on 316L SS properties. Point distance and exposure time were varied and their effect on porosity, surface finish, microstructure, density and hardness, was assessed.

Ma, Wang and Zeng (2015) investigated the microstructural evolution of direct laser deposited IN718 alloy cladding tracks and the effects of energy input (Ev) on microstructural architectures, dendritic morphology, precipitated phases and microhardness.

Carter et al. (2016) studied the SLM process optimization using energy density model for Ni based superalloys, founding that the void area decreases with the increase in energy density (J mm-2).

Li et al. (2019) studied the effect of specific energy density (J/g) on microstructure and corrosion resistance of cobalt-based alloy samples fabricated by LMD. They conclude that the specific energy density reflect the relationship between input energy (W) and feedstock powder (g/s) that have a great effect on solidification microstructure.

From these previous studies can be observed that energy density has major implications on quality geometrical performance (layer height and width) and microstructure (hardness, porosity, cracks, voids) of additive-manufactured parts and samples. Nevertheless, studies for predicting or simulation of this 'energy parameter' performance that affect LMD process chain represents a research line for exploration to reduce and eliminate geometry-related problems and depositions defects, since the LMD process stability is compromised as variations appear during the process execution.

Fuzzy logic (FL) is suitable for modeling complex processes that contain uncertain and vague information with less resources use regarding hardware and software, and has being shown to be an effective technique for addressing linguistically specified goals (Latha and Senthilkumar 2010).

Recent studies applied FL to assess parameters and manufacturing processes performance. Rajamani et al. (2018) studied the wear characteristics prediction of high-density polyethylene samples fabricated by selective inhibition sintering (SIS).

Srivastava et al. (2018) presented a multi-objective fused deposition modeling (FDM) process optimization using RSM embedded FL analysis.

Velázquez et al. (2018); Velázquez (2017) and

Louzada et al. (2016) used FL inference principles to configure the operational design space of a magnetic transducer for biomedical applications, as a foreign object locating system in human body.

Das et al. (2016) developed a grey-fuzzy algorithm to find the process parameters optimal level for CNC milling of Al–4.5%Cu–TiC metal matrix composites.

Supriadi and Manabe (2013) used an adaptive fuzzy controller to enhance the dimensional accuracy of dieless tube-drawing process.

Sahu, Mahapatra and Sood (2013) used FL to develop a study on dimensional accuracy FDM processed parts.

Some other researchers addressed FL principles for studying other manufacturing processes, such as, mold/die polishing sequences (Wu and Wang 2009) and electrical discharge machining (EDM) process with multi-response (Lin and Lin 2005; Lin et al. 2000).

No works were reported yet until this research proposal for studying the application of FL approaches for predicting the effect of LMD process parameter integration on the volumetric energy density (Ev) generated on AISI 316 single-beads deposition. Thus, this study aims to evaluate the behavior of the integration of process parameters laser power - Lp (W), focal length - Fl (mm), laser scan speed - Lss (mm/s) and powder flow - Pf (g/min) on output-variables bead height - Bh (mm) and bead width – Bw (mm), and predict by configuring a FL-based inference system (FIS), the input Ev (J/mm3) generated after deposition of AISI 316 single-beads by LMD process in order to validate a mechanism for guarantee and control the process stability and performance.

2. Materials and Methods

This work was carried out using a hybrid manufacturing system ROMI DCM 620-5X HYBRID that integrates the additive LMD and subtractive 5-axis machining processes. The machine integrates a vertical laser-head with 500 W maximum power Ytterbium Fiber Laser from manufacturer IPG Photonics, 1070 nm wavelength and 1 mm of maximum spot diameter. The system includes another machining-head, which ensures a rotational range of 15-15000 rpm. The dimensions on the X, Y, and Z linear axes are 620x520x460 mm respectively and the rotating table surface on axes B and C is 600x600 mm. Figure 1 shows the configuration of the hybrid machine and its operational axes. Nevertheless, the focus of this study relies on the LMD process as part of preliminary studies to understand how to ensure the process stability.

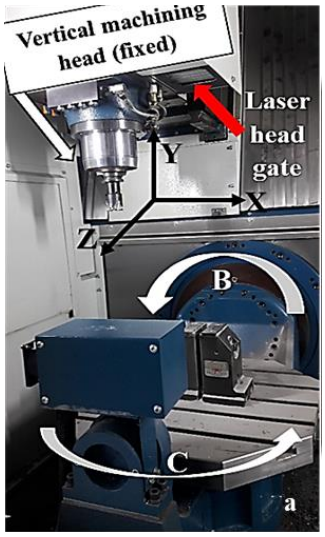

Figure 1. Hybrid System and Operational 5-Axes.

2.1. Process parameters and samples

From previous literature review and after analyzing the deposition and machining system conditions were identified the four process input parameters (Lp (W), Fl (mm), Lss (mm/s), Pf (g/min)) and their operating levels (Table 1) that directly affect the deposition geometrical characteristics, as response-variables (Bh (mm), Bw (mm)). A factorial analysis was performed to determine the better parameter and operating levels possible combinations, resulting in 18 experiments, in order to improve the experimental efforts and assess its interaction's effect on the analyzed variables. Lss (mm/s) parameter was maintained constant and was not included on the factorial analysis.

Table 1. Process Parameter and Operating Levels.

Parameters	Unit	Operating levels		
Lp	W	225	250	275
Lss	mm/s	5	5	5
Pf	g/min	8.95	-	13.42
Fl	mm	4.8	5.0	5.2

The laser beam was focused on the substrate material (AISI 316 SS) to generate 8 single-beads (B1 to B8) on the 18 specimens. The sample dimensions were Ø 25 and 9 mm height, after removing 1 mm of material to ensure the surface flatness. A zig one-way pattern was followed as deposition strategy. The powder used was also AISI 316 SS in the range of 44–106 µm. The length of each single track was 10 mm. The powder was fed simultaneously, by a coaxial hopper focused in the laser-spot with 90° orientation relative to the substrate, with argon gas as a shield.

Figure 2 present the schematic operating configuration that laser beam, shielding gas and powder feed operate regarding the substrate. Figure 3 shows the single-beads characteristics deposited on one sample.

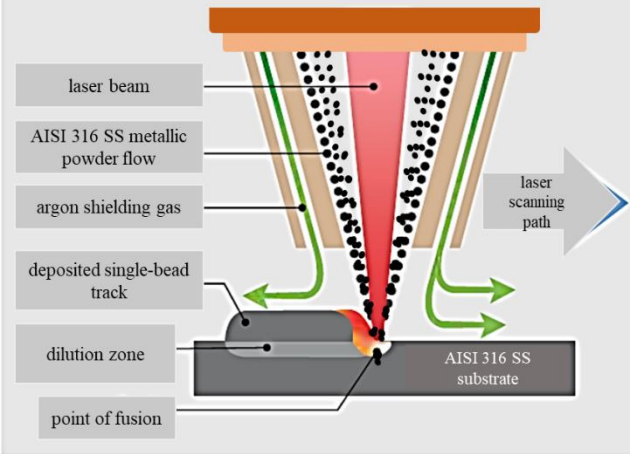

Figure 2. Laser Operational Principle. Adapted from ROMI (2019).

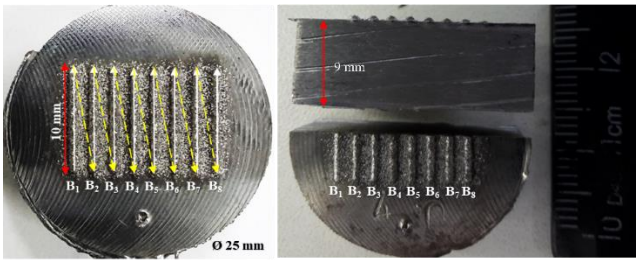

Figure 3. Sample with Deposited Single-Beads Characteristics (left) and Cross-Sectioned sample (right).

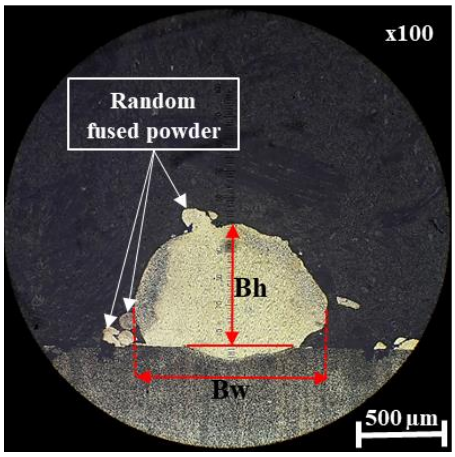

Figure 4. Cross-Sectioned Single-Bead showing the Bh (mm) and Bw (mm)

The specimens were cut in the cross section, Figure 3 (right), and prepared metallographically and them chemically attacked with the reagent Vilela. Bh (mm) and Bw (mm) measurement (Fig. 4) was performed using an optical microscope Nikon Optiphot and lens focus, with 1 mm measurement pattern, was x100.

2.2. FIS for volume energy density prediction

The FIS for Ev (J/mm3) prediction was modeled in Matlab R2011b software on Fuzzy Logic Toolbox. The volumetric energy formula is defined in the Equation 1:

$$Ev\ (J/mm^3) = \frac{Lp\ (W)}{Lss\ (mm/s) * Bh\ (mm) * Bw\ (mm)} \quad (1)$$

When more than one clad is deposited, higher degree of re-melting between over deposited layers (Δz) calls into doubts the use of the bead height (Bh) in the energy density function. The same occurs when there is an overlap rate between deposited neighbor-beads, which the hatch space or beads width (Bw) could come to vary. As a single track was deposited instead more than one continuous layer, no hatch spacing was taken into account for Ev calculus. So, was used in the equation the bead width for volumetric consideration since the laser power has direct influence on beads width, and no over deposited beads could be re-melted.

The structure of the FIS configured in this paper is presented in Figure 5. The development of this predictive FIS involves four subsystems. The first one is the Input data, which are the non-fuzzy data sets corresponding to Lp (W) and Lss (mm/s) operating levels previously defined and Bh (mm), Bw (mm) measurements observations.

The second, is the Fuzzyfication module, which transforms the non-fuzzy data into fuzzy sets (for inputs and outputs) so that they may become instances of input and output linguistic variables. Then, is possible to structure the fuzzy sets and membership functions (MFs) for both inputs and outputs. The MFs used in this paper were the triangular shape as presented in Equation 2:

$$Tiangular\ (x; a, b, c) = \begin{cases} 0, & x \le a \\ \frac{x-a}{b-a}, & a \le x \le b \\ \frac{c-x}{c-b}, & b \le x \le c \\ 0, & c \le x \end{cases} \quad (2)$$

Where, x is a variable (input or output); a, b and c indicate triangular fuzzy triplet of fuzzy sets.

The MFs shape can be defined in Matlab® Membership Functions Editor toolbox for lesser complexity calculation. The 15 fuzzy sets and its MFs structured in this paper are represented in Figure 6. 12 input fuzzy sets and its input MFs corresponds to the input parameters, Figure 6 (a)-(d), and the other three fuzzy set and MFs corresponds to the predicted output volumetric energy density (Ev), Figure 6 (e). The 12 input linguistic variables corresponding to each fuzzy set and MFs (inputs and outputs) were classified as low, medium and high for Lp (W); low, medium and suitable for Bh (mm); small, medium and large for Bw (mm) and, slow, suitable and unsuitable for Lss (mm/s), as seen in Figure 6 (a)-(d), respectively. The output linguistic variables for Ev (J/mm3) were classified as low, medium and high as seen in Figure 6 (e).

Third subsystem is the Fuzzy Inference module, implemented in this paper using the Mamdani (Max-min) inference method (Mamdani and Assilian 1975), which performed a "fuzzy reasoning" from the based-

rules defined to generate a fuzzy value. The Mamdani inference engine determines how rules previously defined following the "if"-"then" constraints are activated for a given situation, combined, and along with input fuzzy data, the module infer the control actions. Fuzzy rules-base (16) structured in this paper are presented in Table 2, codified as: inputs (I = 1, ..., 4) for Lp (W), Bh (mm), Bw (mm) and Lss (mm/s), respectively; MFs and fuzzy sets for each linguistic variable (j = 1, ..., 3) for each input (I); and output (O) for each output MFs, fuzzy sets and linguistic variables (i = 1, ..., 3) representing the Ev (J/mm3) predicted values.

Fourth interface is the Defuzzification method that transforms the information associated with the output linguistic variables into a numeric value (crisp) that can be measured (Saade and Diab 2004). The defuzzyfication method applied here for predicting volumetric energy density Ev (J/mm3) was the so called center of gravity (COG) method (Zimmermann 2001), as following the Equation 3:

$$y_0 = \frac{\sum y \mu_x(y)}{\sum \mu_x(y)} \quad (3)$$

Where, y0 is the defuzzified output of the predicted response variable Ev (J/mm3); y is the variable center value of fuzzy regions and μx(y) the aggregated membership functions. However, the defuzzified output is not needed to be manually calculated since the defuzzyfication method can be selected in Matlab® Fuzzy Logic Editor toolbox.

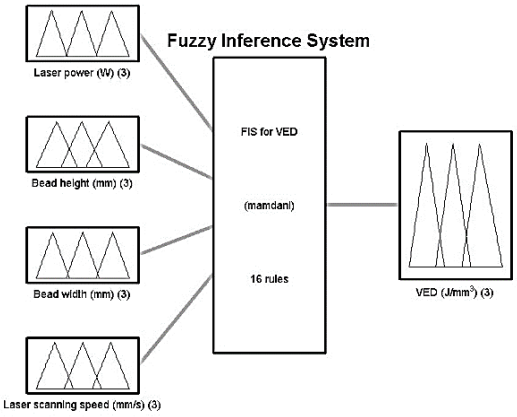

Figure 5. FIS Configuration for Volume Energy Density Ev (J/mm3) Prediction.

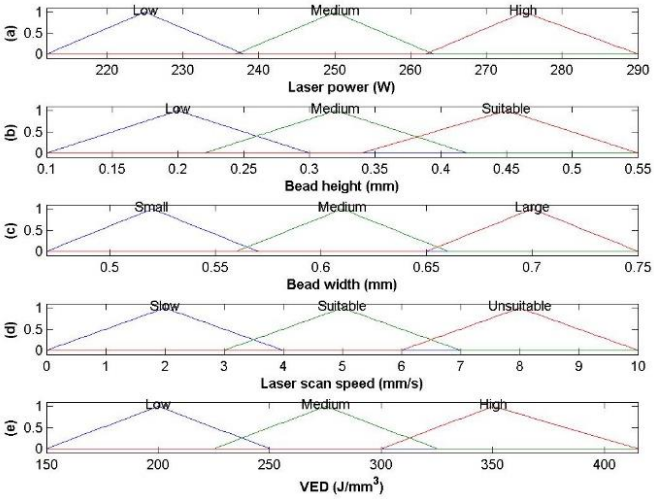

Figure 6. Membership Functions and Fuzzy Sets for: (a)-(d) Input Parameters and, (e) Ev (J/mm3) Output.

Table 2. Fuzzy Rules Base.

Rules	I_j	I_j	I_j	I_j	O_i
1	1_1	2_1	3_1	4_2	O_3
2	1_1	2_2	3_1	4_2	O_3
3	1_1	2_2	3_2	4_2	O_1
4	1_1	2_3	3_2	4_2	O_1
5	1_2	2_1	3_2	4_2	O_2
6	1_2	2_2	3_2	4_2	O_3
7	1_2	2_2	3_3	4_2	O_1
8	1_2	2_3	3_3	4_2	O_1
9	1_3	2_1	3_3	4_2	O_2
10	1_3	2_2	3_3	4_2	O_3
11	1_3	2_3	3_3	4_2	O_1
12	1_2	2_1	3_2	4_2	O_3
13	1_2	2_2	3_2	4_2	O_1
14	1_2	2_3	3_2	4_2	O_1
15	1_3	2_1	3_3	4_2	O_3
16	1_3	2_2	3_3	4_2	O_1

3. Results and Conclusions

Firstly, the effect of the interaction of process parameters on bead height (Bh) and bead width (Bw) was evaluated. Bh and Bw values were observed to increase independently, when the powder flow was higher (13.42 g/min). The greatest height was observed on the experiment 12 at 275 W of Lp, 5 mm of Fl, 5 mm/s of Lss and 13.42 g/min of Pf. The largest width was reached on the experiment 6 at 275 W of Lp, 4.8 mm of Fl, 5 mm/s of Lss and 13.42 g/min. Table 3 summarizes these results.

An ANOVA was used to identify which parameters had significant influence on beads geometrical characteristics Bh and Bw. Tables 4 and 5 present this analysis, reaching P values <0.05 indicate that the parameters' effect on Bh and Bw is significant at a 95 % confidence level. As a result, it is observed on Table 4 that the powder flow (g/min) has greater influence on Bh (mm), and laser power (W) higher signifance on Bw (mm) (Table 5).

Table 3. Experimental, Predicted Values and Error.

Run	Lp (W)	Fl (mm)	Lss (mm/s)	Pf (g/min)	Bh (mm)	Bw (mm)	Ev (J/mm³)		Error %
							Experimental	Fuzzy	
1	225	4,8	5	8,95	0,266	0,516	327,85	353,90	7,36
2				13,42	0,414	0,593	183,30	199,00	7,89
3	250			8,95	0,259	0,603	320,15	318,50	0,52
4				13,42	0,383	0,712	183,35	199,00	7,86
5	275			8,95	0,260	0,662	319,54	318,50	0,33
6				13,42	0,436	0,743	169,78	193,70	12,35
7	225	5		8,95	0,199	0,551	410,40	389,61	5,34
8				13,42	0,400	0,626	179,71	189,69	5,26
9	250			8,95	0,253	0,613	322,40	318,50	1,22
10				13,42	0,392	0,657	194,14	190,90	1,70
11	275			8,95	0,248	0,679	326,62	318,50	2,55
12				13,42	0,454	0,688	176,08	200,00	11,96
13	225	5,2		8,95	0,244	0,528	349,29	354,00	1,30
14				13,42	0,377	0,611	195,36	190,90	2,33
15	250			8,95	0,215	0,606	383,76	353,90	8,44
16				13,42	0,418	0,634	188,67	199,00	5,19
17	275			8,95	0,231	0,686	347,08	353,90	1,93
18				13,42	0,416	0,679	194,72	199,00	2,15

Table 4. ANOVA of Bh (mm) Response for each Source of Variation (Process Parameters).

Source of variation	*SS*	Error	*df*	Error	*MS*	Error	*F*	*P-value*
Laser power (W)	0,0020	0,1292	2	15	0,0010	0,0086	0,1158	*P>0.05*
Powder flow (g/min)	0,1247	0,0065	1	16	0,1247	0,0004	307,0088	*P<0.05*
Focal length (mm)	0,0003	0,1309	2	15	0,0002	0,0087	0,0171	*P>0.05*

Table 5. ANOVA of Bw (mm) Response for each Source of Variation (Process Parameters).

Source of variation	*SS*	Error	*df*	Error	*MS*	Error	*F*	*P-value*
Laser power (W)	0,0311	0,0266	2	15	0,0156	0,0018	8,7570	*P<0.05*
Powder flow (g/min)	0,0098	0,0479	1	16	0,0098	0,0030	3,2881	*P>0.05*
Focal length (mm)	3,5e-05	0,0577	2	15	1,8e-05	0,0038	0,0046	*P>0.05*

Figure 7 presents mean values of Bh (mm) and Bw (mm) for each Lp (W) and Pf (g/min) interactions.

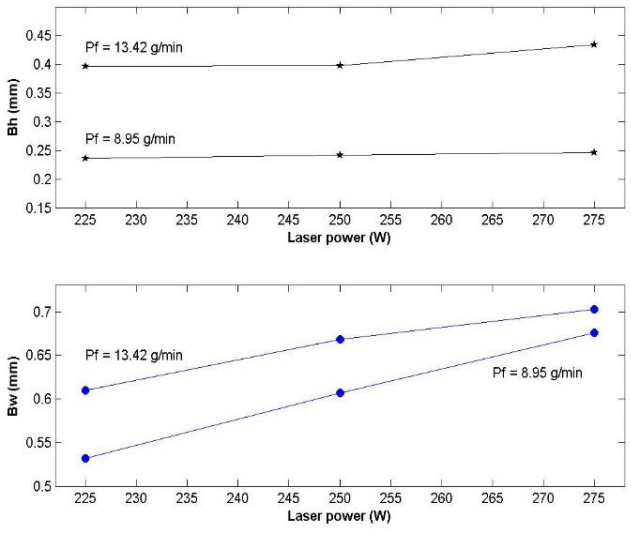

Figure 7. Mean Values of Bh (mm) and Bw (mm) for Lp (W) and Pf (g/min) Interactions.

It was verified when the powder flow increased (g/min), the height of the beads were greater. Therefore, it can be stated that the lower levels of the powder flow affect the height of the beads and the quality of growth of the future layers. The laser power alone does not represent a significant influence on the bead height. Instead, the interaction of the sustained increase in laser power and powder flow has direct impact on the width of the beads.

The results showed on Table 3, Table 4 and Table 5 are in agreement with the works developed by Sun and Hao (2012), Graf et al. (2013), Liu and Kovacevic (2014), Farahmand and Kovacevic (2014), Yu et al. (2018) and Ma, Wang and Zeng (2015).

Sun and Hao (2012) developed a mathematical model for analyzing the influence of laser power, laser advancement speed, and powder flow on Ti6Al4V powder deposition geometry. This analysis indicated that powder flow had a significant effect on the width and height of the coating, while laser-scanning speed had a significant effect on the penetration depth (not assessed in this paper).

Graf et al. (2013) performed a full factorial analysis to determine the effect of process parameters on the cords geometry. They concluded that cords width was typically affected by laser power and the track height is mainly influenced by the deposition velocity and the powder flow. As deposition velocity (in this paper Lss) was not varied, these results were not confirmed.

Liu and Kovacevic (2014), Farahmand and Kovacevic (2014) concluded that the powder flow, the gas flow rate and the interaction between the gas flow rate and the standoff (not assessed) were the most significant factors affecting the bead height, while the laser power was the factor most affects the bead width.

Ma, Wang and Zeng (2015) in their study corroborated that as a result of the orthogonal experiment developed with two factors and four levels that the track width is affected (increase) while increasing laser power (W) and laser speeds (mm/s).

Figure 8 presents the Rules Viewer Toolbox of the Ev (J/mm³) predicted values as result of the experimental procedure performed on the FIS. The Rules Viewer is used to determine each expected output according to each experimental condition executed. The first four columns show the input parameters, and fifth column indicates the output defuzzified response-variable predicted Ev (J/mm³).

For example, by considering the 13th experiment (Table 3), it may be noted that for 225 W of laser power, 0.244 mm of bead height, 0.528 mm of bead width, and 5 mm/s of laser-scanning speed, the output value of the predicted Ev = 354 J/mm³.Predicted Ev, when compared with experimental value obtained (349.29 J/mm3), the relative percentage error is 1.30 %, which can be considered low.

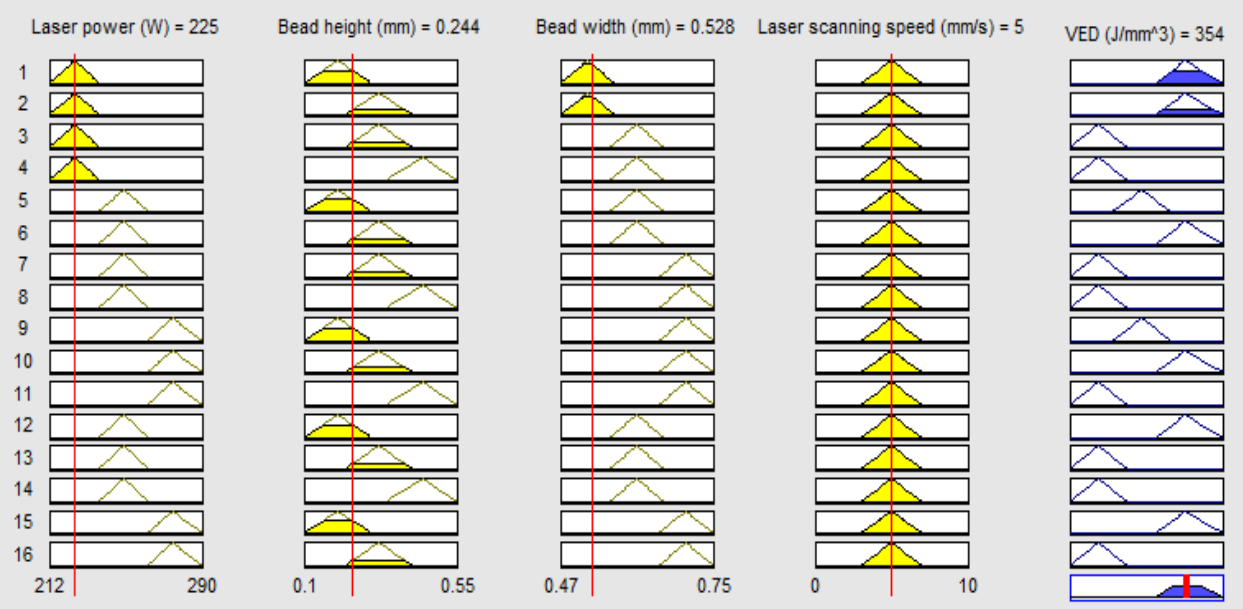

Figure 8. An Rules Viewer Toolbox of Ev (J/mm³) Predicted Values.

Figure 9 presents mean values of Ev (J/mm³) for each Lp (W) and Pf (g/min) interactions.

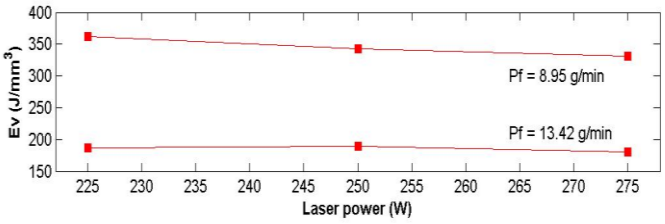

Figure 9. Mean values of Ev (J/mm3) for each Lp (W) and Pf (g/min) interactions.

As the Lss was maintained constantly (5 mm/s) it was observed, that at lower powder flow (8.95 g/min) the average energy density is higher (345.23 J/mm³) and the opposite occurs for higher flow (13.42 g/min), decreasing the average energy (185.01 J/mm³). These results are in agreement with the work of Li et al. (2019) previously discussed. They found that line energy density (J/mm) and specific energy (J/g) increased at constant scanning speed (7 mm/s) reducing the powder feed-rate from 0.941 g/s to 0.327 g/s representing ~34 %, in this paper this variation was ~33 %. However, when increased the laser power (W), the same occurs with the specific energy (J/g).

Different in this paper, while powder flow is lower, but increasing the laser power from 225 W, 250 W and 275 W, the mean Ev decrease from 362.52 J/mm³ to 342.10 J/mm³ and 331.08 J/mm³, respectively. Higher powder flow, at the three laser power levels, the mean Ev presents a decreasing variation between 186.12 J/mm³ until 180.19 J/mm³, however a lighter

increasing at 250 W was measured (188.72 J/mm³). These variations occur because in the energy formula was used the Bw (mm) instead hatch spacing (mm), as it was deposited only a single bead and not multiple layers as in Li et al. (2019). So, as showed in Table 5, Lp (w) has direct influence on Bw (mm), therefore, increasing the power generates larger width.

The results of our study are also confirmed when compared with Ma, Wang and Zeng (2015) work. In their energy input analysis they kept constant the layer thickness – h (mm) but varying in four levels the laser power - P (W), the laser speed –V (mm/s) and the width of the cladding track – d (mm). Their results showed that for different increased levels of overlap rate (%) between two neighbor-deposited clads while also increasing P (W), V (mm/s) and d (mm) the Ev (J/mm3) decreased. The opposite occurs when higher overlap rates are used but maintaining constant the other parameters, so it means that one clad is deposited nearly above the other one, so width tends to be reduced and while P (W) doubles consequently the Ev increases.

Figure 10 and Figure 11 present the 3D contour surface profile of the inputs interactions, such as, laser power, bead height, and bead width as results of the predictive fuzzy Ev modeling. Figure 10 shows the interface between laser power (W) and bead height (mm); and Figure 11, for laser power and bead width. The region with strongest colored contour indicates higher Ev predicted values.

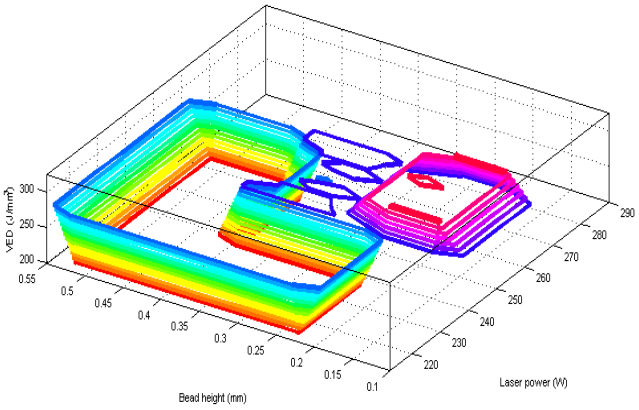

Figure 10. 3D Contoured Surface of Predicted Ev (J/mm3) Values for Lp (W) and Bh (mm) Interaction.

Comparative evaluation between fuzzy based inference system and experiments was carried out and depicted in Figure 12. It is observed that good correlation exists between them and average error of volumetric energy is found to be 4.76 % which is very low considering the number of experiments carried out. Therefore, the proposed results show that the fuzzy inference model based on the Mamdani method provides an adequate prediction of the evaluated output variable Ev (J/mm3).

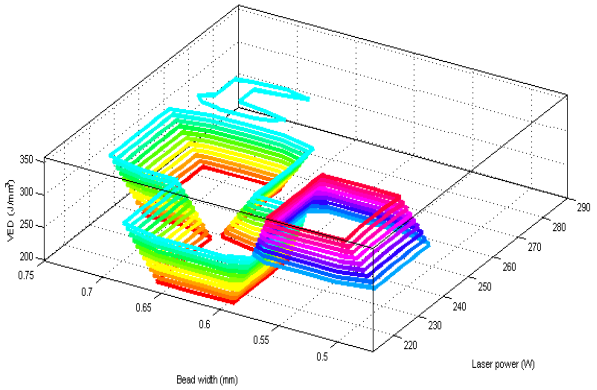

Figure 11. 3D Contoured Surface of Predicted Ev (J/mm3) Values for Lp (W) and Bw (mm) Interaction

.

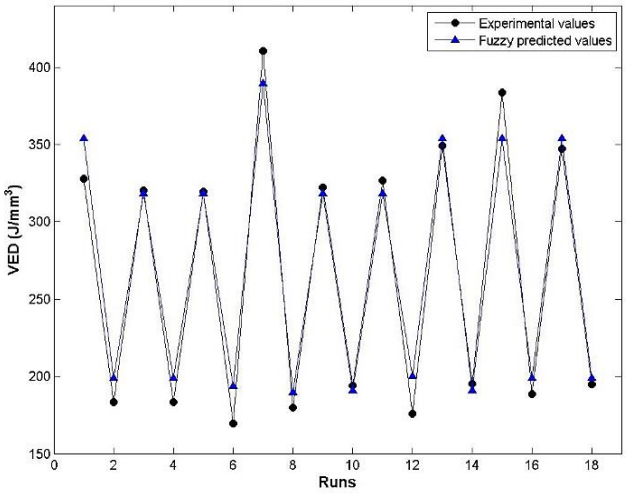

Figure 12. Correlation between Experimental and Fuzzy Predicted Values of Ev (J/mm3)

4. Conclusions

In this paper, a fuzzy inference-based modeling was developed for predicting the volumetric energy input Ev (J/mm3) on single AISI316 SS beads deposited by LMD additive manufacturing process. Taking into account the different process parameter operating levels, a factorial analysis-based DoE was performed for identify all possible process parameters combination to optimize process performance analysis. First of all, the effect of laser power (W), focal length (mm), powder flow (g/min) and laser scan speed (mm/s) process parameters on single beads height (mm) and width (mm) were individually evaluated. The greatest track height was 0.454 mm and the largest width was 0.743 mm. The higher energy input was reached for 410.4 J/mm3 on the 7th experiment at 225 W of laser power, 5 mm of focal length, 8.95 g/min of powder flow, 5 mm/s of laser scan speed, 0.199 mm of bead height and 0.551 mm of bead width. The lower Ev was reached on the 6th for 169.78 J/mm3. ANOVA indicated that powder flow has a significant effect on Bh, and in lower manner the laser power and focal length. While on Bw, laser power has the greatest influence. The predictive fuzzy

inference modeling outputs are validated with the experimental data, which was highly satisfactory presenting a good correlation index in terms of the average percentage error of 4.76 %. Future research could focus on studying the influence of the energy density on beads dilution and deep of penetration on the substrate.

Funding and Acknowledgements

The authors thanks to the Higher Education Personnel Improvement Coordination – Brazil (CAPES - Coordenação de Aperfeiçoamento de Pessoal de Nível Superior) which financed this study in part - Finance Code 001, and thanks to ROMI Industry for allowing the open and wide access to its facilities.

References

Amine T., Newkirk J.W., Liou F., 2014. An investigation of the effect of laser deposition parameters on characteristics of multilayered 316L deposits. International Journal of Advanced Manufacturing Technology, 73, 1739–1749.

Ansari M., Mohamadizadeh A., Huang Y., Paserin V., Toyserkani, E., 2019. Laser directed energy deposition of water-atomized iron powder: Process optimization and microstructure of single-tracks. Optics & Laser Technology, 112, 485-493.

Arrizubieta J., Aitzol L., Magdalena C., Eneko U., Amaia A., 2018. Hardness, grainsize and porosity formation prediction on the Laser Metal Deposition of AISI 304 stainless steel. International Journal of Machine Tools and Manufacture, 135, 53–64.

Carter L.N., Wang X., Read N., Khan R., Aristizabal M., Essa K., Attallah M.M., 2016. Process optimisation of selective laser melting using energy density model for nickel based superalloys. Materials Science and Technology, 32 (7), 657-661.

Cherry J.A., Davies H.M., Mehmood S., Lavery N.P., Brown S.G.R., Sienz J., 2014. Investigation into the effect of process parameters on microstructural and physical properties of 316L stainless steel parts by selective laser melting. The International Journal of Advanced Manufacturing Technology, 76 (5–8), 869–79.

Das B., Roy S., Rai R.N., Saha S.C., 2016. Application of grey fuzzy logic for the optimization of CNC milling parameters for Al–4.5%Cu–TiC MMCs with multi-performance characteristics. Engineering Science and Technology, an International Journal, 19 (2), 857-865.

Farahmand P., Kovacevic R., 2014. Parametric study and multicriteria optimization in laser cladding by a high power direct diode laser. Lasers in Manufacturing and Materials Processing, 1, 1–20.

Graf B., Ammer S., Gumenyuk A., Rethmeier M., 2013. Design of experiments for laser metal deposition in maintenance, repair and overhaul applications. Procedia CIRP, 11, 245–248.

Huang Y., Ansari M., Asgari H., Hossein M., Farshidianfar M.H., Sarker D., Khamesee M.B., Toyserkani E., 2019. Rapid prediction of real-time thermal characteristics, solidification parameters and microstructure in laser directed energy deposition (powder-fed additive manufacturing). Journal of Materials Processing Technology, 274, 116286.

Latha B., Senthilkumar V.S., 2010. Modeling and analysis of surface roughness parameters in drilling GFRP composites using fuzzy logic. Materials and Manufacturing Processes, 25 (8), 817–827.

Li J., Ren H., Liu C., Shang Sh., 2019. The Effect of Specific Energy Density on Microstructure and Corrosion Resistance of CoCrMo Alloy Fabricated by Laser Metal Deposition. Materials, 12, 1321.

Lin J.L., Lin C.L., 2005. The use of grey-fuzzy logic for the optimization of the manufacturing process. Journal of Materials Processing Technology, 160 (1), 9-14.

Lin J.L., Wang K.S., Yan B.H., Tarng Y.S., 2000. Optimization of the electrical discharge machining process based on the Taguchi method with fuzzy logics. Journal of Materials Processing Technology, 102 (1–3), 48-55.

Liu S., Kovacevic R., 2014. Statistical analysis and optimization of processing parameters in high-power direct diode laser cladding. The International Journal of Advanced Manufacturing Technology, 74, 867–878.

Louzada D.R., Monteiro E.C., Fortaleza L.G.S., Barbosa C.R.H., Velázquez D.R.T., Silva E.C., Gusmão L.A.P., 2016. Quality by Design approach in the development of a magnetic transducer for biomedical measurements: Preliminary results on Design Space configuration. Journal of Physics: Conference Series, 772, 1-6.

Ma M., Wang Z., Zeng X., 2015. Effect of energy input on microstructural evolution of direct laser fabricated IN718 alloy. Materials Characterization, 106, 420–427.

Rajamani D., Esakki B., Arunkumar P., Velu R., 2018. Fuzzy logic-based expert system for prediction of wear rate in selective inhibition sintered HDPE parts. Materials Today: Proceedings, 5, 6072–6081.

Romi. ROMI DCM 620-5X HYBRID Technical specifications. Available in: https://www.romi.com/wp-content/uploads/2017/10/fol_romi_dcm_hybrid_po_aa_052017_baixa.pdf. Access February 2019.

Saade J.J., Diab H.B., 2004. Defuzzification methods and new techniques for fuzzy controllers. Iranian Journal of Electrical and Computer Engineering, 3,

161-174.

Sahu R.K., Mahapatra S.S., Sood A.K., 2013. A study on dimensional accuracy of fused deposition modelling (FDM) processed parts using fuzzy logic. Journal for Manufacturing Science and Production, 13 (3), 183 – 197.

Schmidt M., Merklein M., Bourell D., Dimitrov D., Hausotte T., Wegener, K., Overmeyer, L., Vollertsen, F., Levy, G.N., 2017. Laser based additive manufacturing in industry and academia. CIRP Annals - Manufacturing Technology, 66 (2), 561–583.

Srivastava M., Rathee S., Maheshwari S., Kundra T.K., 2018. Multi-objective optimization of fused deposition modelling process parameters using RSM and fuzzy logic for build time and support material. International Journal of Rapid Manufacturing, 7 (1), 25–42.

Supriadi S., Manabe K., 2013. Enhancement of dimensional accuracy of dieless tube-drawing process with vision-based fuzzy control. Journal of Materials Processing Technology, 213 (6), 905-912.

Thijs L., Verhaeghe F., Craeghs T., Humbeeck J., Kruth J-P., 2010. A study of the microstructural evolution during selective laser melting of Ti–6Al–4V. Acta Materialia, 58, 3303–3312.

Velázquez D.R.T., 2017. Quality by Design Fuzzy multi-paramétrico no desenvolvimento de sistema de medição para uso clínico. Dissertation (MSc) – Pontifícia Universidade Católica do Rio de Janeiro.

Velázquez D.R.T., Louzada D.R., Monteiro E.C., Fortaleza L.G.S., Barbosa C.R.H., Silva E.C., Gusmão L.A.P., 2018. Multi-parameter fuzzy design space for QbD approach applied in the development of biomedical devices. Journal of Physics: Conference Series, 1044, 1-6.

Wei K., Gao M., Wang Z., Zeng X., 2014. Effect of energy input on formability, microstructure and mechanical properties of selective laser melted AZ91D magnesium alloy. Materials Science & Engineering, A611, 212–222.

Wu B.H., Wang J-J.J., 2009. A neuro-fuzzy approach to generating mold/die polishing sequences. Journal of Materials Processing Technology, 209 (7), 3241-3250.

Wu J., Liu T., Chen H., Lia F., Wei H., Zhang Y., 2019. Simulation of laser attenuation and heat transport during direct metal deposition considering beam profile. Journal of Materials Processing Technology, 270, 92–105.

Yu T., Zhao Y., Sun J., Chen Y., Qu W., 2018. Process parameters optimization and mechanical properties of forming parts by direct laser fabrication of YCF101 alloy. Journal of Materials Processing Technology, 262, 75-84.

Zimmermann, H.-J., 2001. Fuzzy set theory and its applications. 4th ed. Springer Science + Business Media New York.